

## $4\sigma^{-1}$ Inner Valence Photoionization Dynamics of NO Derived from Photoelectron-Photoion Angular Correlations

O. Geßner,<sup>1</sup> Y. Hikosaka,<sup>2</sup> B. Zimmermann,<sup>1,\*</sup> A. Hempelmann,<sup>1</sup> R. R. Lucchese,<sup>3</sup>  
J. H. D. Eland,<sup>4</sup> P.-M. Guyon,<sup>5</sup> and U. Becker<sup>1</sup>

<sup>1</sup>*Fritz-Haber-Institut der Max-Planck-Gesellschaft, Faradayweg 4-6, 14195 Berlin, Germany*

<sup>2</sup>*Photon Factory, Institute of Materials Structure Science, KEK, Tsukuba, 305-0801, Japan*

<sup>3</sup>*Texas A&M University, Department of Chemistry, College Station, Texas 77842-3012*

<sup>4</sup>*Physical & Theoretical Chemistry Laboratory, South Parks Road, Oxford OX1 3QZ, United Kingdom*

<sup>5</sup>*Laboratoire des Collisions Atomiques et Moléculaire Bâtiment 351, Université Paris Sud, 91405 Orsay, France*

(Received 4 February 2002; published 30 April 2002)

A complete description of the  $4\sigma$  photoionization dynamics of NO has been derived from angle resolved photoelectron-photoion-coincidence experiments. The combination of measurements performed with linearly and circularly polarized light has made it possible to obtain a unique set of complex dipole matrix elements. A comparison with multichannel-Schwinger-configuration-interaction calculations shows good agreement in the general shapes of the angular distributions due to the correct description of the main components and phase differences. Still, many transition moments agree only qualitatively.

DOI: 10.1103/PhysRevLett.88.193002

PACS numbers: 33.60.Cv, 33.80.Gj

Molecule frame angular distributions of photoelectrons display the dynamics of the molecular photoionization process in the most direct way and have therefore been studied theoretically for many years [1–4]. But only within the last 10 years, gas phase studies of the vector correlations between the orientation of the molecular axis in space and the outgoing photoelectron momentum have become experimentally feasible by various photoelectron-photoion coincidence methods [5–10]. All of these methods make use of the so-called “axial-recoil-approximation”: if the dissociation of a molecule after photoionization is fast compared to its rotational time scale, one can derive the molecular axis orientation in space by measuring the momentum vectors of the molecular fragments [11]. The formulas to derive a complete description of the molecular photoionization process, by the analysis of fixed-in-space molecules photoelectron angular distributions, were given about 25 years ago by Dill [1]. Several publications consider the feasibility of complete experiments on the basis of these formulas [12] and experimental approaches to implement this idea [6,13–17]. The most recent articles [16,17] emphasize the necessity of using linearly and circularly polarized light in order to derive all matrix elements and phase shifts including their signs. For the special case of rotationally resolved ( $1 + 1'$ ) resonance-enhanced multiphoton ionization (REMPI) measurements, the feasibility of a complete experiment was shown by Reid *et al.* [18] and discussed by Leahy *et al.* [19]. Still, to our knowledge there is no derivation of all dipole transition parameters for the direct, rotationally unresolved photoionization of a heteronuclear diatomic molecule by a sufficiently reliable fit only, without using any further assumptions derived by *ab initio* calculations. The main problem was that no combined data resulting from both types of polarization were available. In this Letter we report the first complete description of the  $4\sigma^{-1}$

inner valence photoionization of NO molecules derived solely from experimental data. We used 13 independent parameters: 7 dipole transition moments and 6 phase differences. The combined angular distribution and circular dichroism data provide, for the first time, the basis to derive a reliability estimation for the fitting results by means of standard fit probability functions. The measured data and the derived dipole transition parameters are compared to multichannel Schwinger configuration interaction (MCSCI) calculations [20,21].

The data were taken in two independent measurements, one using linearly, the other circularly polarized light of two opposite helicities with a photon energy of 40.8 eV. We investigated the  $4\sigma^{-1}$  photoemission corresponding to the excitation into the  $c^3\Pi$  state of  $\text{NO}^+$  which subsequently dissociates into a  $\text{N}^+(^3P)$  ion and neutral  $\text{O}(^3P)$  atom. For the *linear polarization measurements*, a monochromized helium discharge lamp was used as the light source. The degree of linear polarization was  $p_1 = 0.35$ , while  $p_2$  and  $p_3$  were negligible. The Stokes parameters used in this article follow the definition given in [22]. Electrons and ions were extracted in opposite directions by constant electric fields and detected using time- and position-sensitive detectors placed opposite to each other with their common axis oriented perpendicular to the plane defined by the electric vector of light and the light propagation direction. Details are described elsewhere [8]. With this setup we measured the  $4\sigma^{-1}$  photoelectron angular distributions (PEADs) for all orientations of the molecular axis relative to the electric vector of light simultaneously. For the analysis, the molecular axis and the electron emission direction were selected to be coplanar with the electric vector of light and the light propagation direction. The *circular polarization measurements* were performed at the U2-FSGM beam line [23] at the synchrotron light source BESSY I. The

degree of circular polarization was  $|p_3| = 0.3 \pm 0.1$ , while  $p_1$  and  $p_2$  were negligible. The sign of  $p_3$  was derived from previous measurements and [24]. The electrons were detected in 5 independent time-of-flight (TOF) analyzers with a small entrance aperture which detected only electrons emitted in the plane perpendicular to the light propagation direction. The detection of an electron triggered a high voltage extraction pulse for the ions which were detected on a time- and position-sensitive detector. Details are described elsewhere [25]. With this setup we measured the  $N^+$  photoion angular distributions (PIADs) relative to the emission direction of the  $4\sigma^{-1}$  photoelectrons in the plane perpendicular to the light propagation direction. In this measuring plane the  $N^+$  PIADs for fixed  $4\sigma^{-1}$  electron emission directions are equivalent to the  $4\sigma^{-1}$  PEADs for fixed  $N^+$  ion emission directions, provided that the light does not have any contributions from  $p_1$  or  $p_2$ . The only difference is a change in the sign of the angular frames when swapping from electrons to ions. In the experiment with linear polarization, the angular resolutions (FWHM, including the effects of binning the data) were  $29^\circ$  for ions,  $14^\circ$  for electrons in the measuring plane, and  $96^\circ$  (ions) and  $48^\circ$  (electrons) perpendicular to that plane. In the experiment with circular polarization the angular resolutions (FWHM) were  $34^\circ$  for ions,  $8^\circ$  for electrons, in both planes. To analyze the data we used a parametrization of the angular correlations of the molecular orientation in space, the electron emission direction, and the state of light [26]. Although there are already a number of parametrizations of the molecular photoionization process [1,2] we derived an easy-to-use one [26] in the formalism of the density matrix theory [27]. It has the general form

$$I(\underline{\kappa}, \underline{m}) = C \sum_{d\mathcal{L}\Gamma} M_{d\mathcal{L}\Gamma} F_{d\mathcal{L}\Gamma}, \quad (1)$$

with  $C$  = normalization factor,  $\underline{\kappa}$  = photoelectron momentum vector,  $\underline{m}$  = orientation vector of the molecular axis in space. While the coefficients  $M_{d\mathcal{L}\Gamma}$  contain only information about the dynamics as functions of dipole transition moments and phase differences, the  $F_{d\mathcal{L}\Gamma}$  reflect the geometrical arrangement and the state of light only [26]. Although the angular momentum quantum number  $l$  is unlimited in the partial wave expansion of the outgoing electron wave, the expansion converges very quickly for higher  $l$ . The restriction to contributions from outgoing partial waves with  $l \leq l_{\max}$  is the approximation within which we call our experiment complete (within the dipole approximation). The value of  $l_{\max}$  has to be derived from the fitting results. The application of Eq. (1) to particular geometries and light polarization states can lead to relatively simple equations, for example the well known  $\beta$  formula [28] or the expansions to Legendre polynomials as given in [1,12]. The coefficients  $M_{d\mathcal{L}\Gamma}$  have to fulfill constraints corresponding to the dipole approximation and symmetry restrictions [6,26]. Fitting the  $M_{d\mathcal{L}\Gamma}$  with-

out caring about the constraints can lead to nonphysical results. By using a fitting procedure which directly fits the transition moments and phase shifts to the experimental data using Eq. (1) the constraints are automatically fulfilled. Besides the fact that this opens the way to analyze the reliability of the fit results using general probability functions, another important analysis step becomes feasible. This is the inclusion of all experimental deviations from the ideal symmetry restrictions due to finite angular resolutions. The inclusion of the finite angular resolution for both electrons and ions, in both angular dimensions, in the measuring plane and perpendicular to it, is a crucial point in the analysis.

Figure 1 shows our results for the case of excitation using linearly polarized light. The excellent agreement between the data and the fit is shown by three showcase examples for excitation angles of  $0^\circ$ ,  $45^\circ$ , and  $90^\circ$ .

Figure 2 shows the  $N^+$  ion angular distributions relative to the photoelectron emission direction for the two different light helicities, and the circular dichroism in the angular distribution (CDAD) which is the difference between the intensities. The solid curve in the CDAD graph represents the same set of dipole transition moments and phase shifts as the solid curves in Fig. 1. The dotted curve is the output of the MCSCI calculations which is in qualitatively good agreement with the measurements.

To prove the reliability of the fitting procedure and the results with particular respect to the different angular resolutions in the two experiments, we performed two kinds of fits. First we fitted all data for linear and circular polarization simultaneously. Second, we performed the fits for the linear and the circular polarization data sets independently. The set of parameters yielding a reasonable fit for both data sets is exactly the same as in the simultaneous fit. This shows that the lower angular resolution of

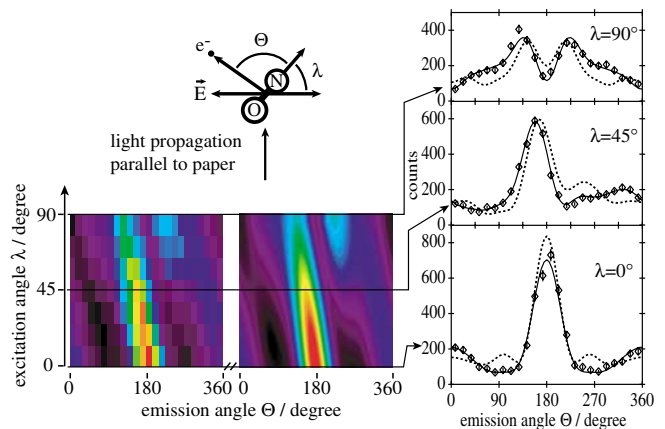


FIG. 1 (color).  $4\sigma^{-1}$  photoelectron angular distributions for a series of excitation geometries using linearly polarized light. The color maps show the data (left-hand side) and the fit (right-hand side), respectively. The Cartesian plots to the right are cuts through the maps at three different excitation angles. Solid line: fit; dotted line: MCSCI (convoluted with experimental angular resolution).

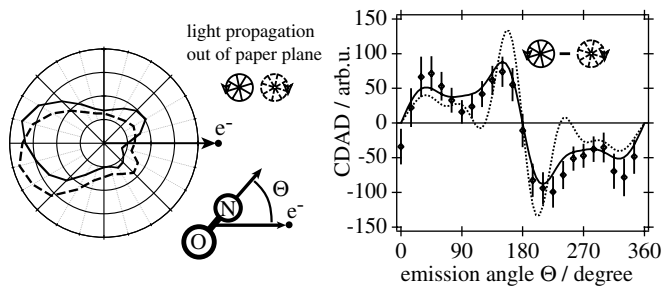


FIG. 2. Left:  $N^+$  ion angular distributions relative to the  $4\sigma^{-1}$  photoelectron emission direction using circularly polarized light of two opposite helicities. Solid line:  $E$ -vector rotates counterclockwise (positive helicity); dashed line:  $E$ -vector rotates clockwise (negative helicity) when facing the light beam. Right: CDAD of the  $N^+$  ion emission. Solid line: fit; dotted line: MCSCI (convoluted with experimental angular resolution).

the linear polarization measurement does not hide any features because they would show up in the, in this respect, more sensitive circular dichroism experiment with the better overall angular resolution. This indicates that both data sets are equally suited for the partial wave analysis of the system under investigation. The fitting procedure was performed for  $l_{\max} = 1, \dots, 5$ . The quality of the fit does not increase beyond  $l_{\max} = 3$  while  $l_{\max} = 2$  does not yield satisfactory fit results. This is on a first glance surprising, but strongly corroborated by the MCSCI calculations, which show that all components with  $l > 3$  have only marginal effect on the angular distributions. Thus we describe the process within the approximation  $l_{\max} = 3$ . Fits were performed for approximately 20000 sets of random generated starting values.

Table I shows the parameter sets for the best and the second best fit results, along with the results of the MCSCI calculations. While the dipole transition moment ratios are the result of the fit, the absolute transition cross sections given in Table I were derived using the absolute cross sections of the  $4\sigma^{-1}$  photoline measured by Gustaffson *et al.* [29] for normalization. The extrapolation from their high-

est 40 eV to our 40.8 eV photon energy was done using the calculations of Smith *et al.* [30]. The phase differences are shifted to  $\delta_{s\sigma} = 0$ . The reason why the two best solutions are shown in Table I is the following: a fit to a complex function using 13 fit parameters can lead to a variety of local minima in the multidimensional parameter space when the starting values are varied. One way to define a unique solution of the fit is to take the global minimum and to neglect all other minima. This makes sense if all but the global minimum are obviously wrong solutions in terms of an eye guided quality check of the fit. The major disadvantage of this method is that it is very observer dependent and the qualities of different fits are hard to compare. Therefore we used a purely mathematical way to estimate the reliability of different fit results. Provided that the error bars of a data set of  $n$  points are purely statistical, the probability of a certain  $\chi^2$  of the fit when describing the data set with the correct model of  $m$  fit parameters can be calculated from  $n$ ,  $m$ , and  $\chi^2$  [31]. Vice versa, by integrating the probability functions given in [31] we can estimate the reliability of our fitting results as a function of their  $\chi^2$ . Applying this method, the probability of the best fit is 10 times higher than the one of the second best fit. All other parameter sets found by the fit routine show a fit quality which is at least 100 times less probable than the one of the best fit. The error bars for the two parameter sets were derived by shifting every single parameter  $q_i$  slightly from its optimal value by  $\Delta q_i$  and then performing the fit again with the varied parameter kept constant. The standard deviation  $\sigma(q_i)$  for each parameter  $q_i$  is estimated by  $\sigma(q_i) = \frac{\Delta q_i}{\Delta \chi^2}$  where  $\Delta \chi^2$  is the variation of  $\chi^2$  compared to the best result [31]. Note that our best fit result points to a vanishing or very small phase difference between the  $\sigma$  and the  $\pi$  continua of each partial wave.

From Table I one can see that the MCSCI calculations which describe the general features in the angular distributions and the CDAD in Figs. 1 and 2 quite well, do

TABLE I. Dipole transition moments ( $d$  in  $1/\sqrt{\text{a.u.}}$ ) and phase differences ( $\delta$  in rad) for the best solution (A), the second best solution (B), and the MCSCI calculation (th). All  $\delta$  relative to  $\delta_{s\sigma} \equiv 0$ . The errors do not include the uncertainty of the absolute cross section  $\sigma = 1.52 \text{ Mb}$ .

	$l = 0$	$l = 1$	$l = 2$	$l = 3$	
$d_{l\sigma}$	$0.071 \pm 0.007$	$0.211 \pm 0.013$	$0.276 \pm 0.011$	$0.103 \pm 0.009$	(A)
	$0.202 \pm 0.010$	$0.186 \pm 0.012$	$0.240 \pm 0.012$	$0.044 \pm 0.014$	(B)
	0.173	0.135	0.339	0.234	(th)
$\delta_{l\sigma}$	0	$0.13 \pm 0.10$	$3.66 \pm 0.11$	$1.46 \pm 0.17$	(A)
	0	$3.01 \pm 0.07$	$1.87 \pm 0.08$	$5.8 \pm 0.3$	(B)
	0	1.157	4.977	3.343	(th)
$d_{l\pi}$	...	$0.115 \pm 0.006$	$0.285 \pm 0.011$	$0.162 \pm 0.010$	(A)
	...	$0.291 \pm 0.012$	$0.089 \pm 0.012$	$0.168 \pm 0.010$	(B)
	...	0.052	0.191	0.252	(th)
$\delta_{l\pi}$	...	$0.09 \pm 0.12$	$3.65 \pm 0.11$	$0.82 \pm 0.12$	(A)
	...	$3.4 \pm 0.2$	$0.82 \pm 0.18$	$5.59 \pm 0.12$	(B)
	...	5.907	4.459	1.679	(th)

TABLE II. Measured and calculated integrated molecular excitation and photoelectron emission asymmetry parameters.

	Derived from coincidence data fit	Independent measurement	MCSCI calculation
$\beta_m$	$0.08 \pm 0.06$	$0.14 \pm 0.05$	0.543
$\beta_e$	$1.23 \pm 0.05$	$1.11 \pm 0.11$	0.514

not agree quantitatively with most of the transition moments and phase differences. However, a closer look to the theoretical data reveals that the identification of the major even component ( $l = 2$ ), its small relative phase shift between the  $d\sigma$  and the  $d\pi$  continua, and the relative phase shift to the neighboring odd components ( $\delta_{2\sigma} - \delta_{1\sigma}$  and  $\delta_{2\pi} - \delta_{3\pi}$ ) agree well with the experiment.

In the calculations we used the same 17 channel calculation as was used previously to study molecular frame photoelectron angular distributions for ionization leading to the  $c^3\Pi$  state of  $\text{NO}^+$  [32]. The 17 states of  $\text{NO}^+$  in the scattering wave function included the 12 states listed in Table I of Ref. [21] and five higher energy states that lead to the inclusion of important correlation terms.

A further important cross check of the results is the comparison to independently derived quantities. We measured the anisotropy parameters  $\beta_m$  and  $\beta_e$  of the integrated ion- and electron-angular distributions, respectively, using noncoincident methods. The comparison of these measurements with the values derived from our best fit result of transition matrix elements and phase shifts are shown in Table II. The agreement is very good within the error bars of both measurements.

In conclusion, we have measured the molecule frame angular distributions of photoelectrons and photoions emitted after the  $4\sigma^{-1}$  photoionization of NO molecules in the gas phase. At a photon energy of 40.8 eV we used both linearly and circularly polarized light to derive a unique set of dipole transition moments and phase differences describing the measurements very accurately with 13 parameters corresponding to a maximum angular momentum quantum number  $l_{\max} = 3$  of the outgoing photoelectron partial waves. The comprehensive data set and the good agreement with the fit provide theoreticians with a showcase example for the inner valence photoionization of an open shell molecule. The comparison to MCSCI calculations in the fixed nuclei approximation shows the capability of this method to predict the general features of the angular distributions due to the correct identification of the main components of the photoelectron wave expansion including their relative phase shifts.

This work was in part supported by the Welch Foundation under Grant No. A-1020, by the Texas A&M University Supercomputing Facility, and by the Deutsche Forschungsgemeinschaft under Grant No. Be 860/14-2. We also thank the EPSRC for financial support and the staff at BESSY. P.M.G. acknowledges support from the Human Capital and Mobility Program of the European

Community. B.Z. likes to thank the Alexander von Humboldt Foundation, Germany, for the Feodor Lynen Research award.

\*Present address: California Institute of Technology, 1200 East California Boulevard, MC 127-72 Pasadena, CA 91125.

- [1] D. Dill, *J. Chem. Phys.* **65**, 1130 (1976).
- [2] N. A. Cherepkov and V. V. Kuznetsov, *Z. Phys. D* **7**, 271 (1987).
- [3] J. W. Davenport, *Phys. Rev. Lett.* **36**, 945 (1976).
- [4] R. L. Dubs, S. N. Dixit, and V. McKoy, *Phys. Rev. Lett.* **54**, 1249 (1985).
- [5] A. V. Golovin, *Opt. Spectrosc. (USSR)* **71**, 537 (1991).
- [6] S. Motoki *et al.*, *J. Phys. B* **33**, 4193 (2000).
- [7] F. Heiser *et al.*, *Phys. Rev. Lett.* **79**, 2435 (1997).
- [8] M. Takahashi, J. P. Cave, and J. H. D. Eland, *Rev. Sci. Instrum.* **71**, 1337 (2000).
- [9] A. Landers *et al.*, *Phys. Rev. Lett.* **87**, 013002 (2001).
- [10] A. Lafosse *et al.*, *Phys. Rev. Lett.* **84**, 5987 (2000).
- [11] R. N. Zare, *J. Chem. Phys.* **47**, 204 (1967).
- [12] N. A. Cherepkov *et al.*, *J. Phys. B* **33**, 4213 (2000).
- [13] E. Shigemasa *et al.*, *Phys. Rev. Lett.* **80**, 1622 (1998).
- [14] Y. Hikosaka and J. H. D. Eland, *J. Phys. B* **33**, 3137 (2000).
- [15] O. Gessner *et al.*, *J. Electron. Spectrosc. Relat. Phenom.* **101–103**, 113 (1999).
- [16] S. Motoki *et al.*, *Phys. Rev. Lett.* **88**, 063003 (2002).
- [17] T. Jahnke *et al.*, *Phys. Rev. Lett.* **88**, 073002 (2002).
- [18] K. L. Reid, D. J. Leahy, and R. N. Zare, *Phys. Rev. Lett.* **68**, 3527 (1992).
- [19] D. Leahy, K. Reid, H. Park, and R. N. Zare, *J. Chem. Phys.* **97**, 4948 (1992).
- [20] R. E. Stratmann and R. R. Lucchese, *J. Chem. Phys.* **102**, 8493 (1995).
- [21] R. E. Stratmann, R. W. Zurales, and R. R. Lucchese, *J. Chem. Phys.* **104**, 8989 (1996).
- [22] H. Klar and H. Kleinpoppen, *J. Phys. B* **15**, 933 (1982).
- [23] R. David *et al.*, *Nucl. Instrum. Methods Phys. Res., Sect. A* **343**, 650 (1994).
- [24] W. B. Peatman *et al.*, in Annual Report of the Berliner Elektronenspeicherring-Gesellschaft für Synchrotronstrahlung mbH (BESSY) 1992, p. 499, and references therein.
- [25] U. Becker, O. Gessner, and A. Rüdél, *J. Electron Spectrosc. Relat. Phenom.* **108**, 189 (2000).
- [26] B. Zimmermann, *Vollständige Experimente in der atomaren und molekularen Photoionisation* in Studies of Vacuum Ultraviolet and X-ray Processes, edited by U. Becker (Wissenschaft und Technik Verlag, Berlin, 2000), Vol. 13, p. 130.
- [27] K. Blum, *Density Matrix Theory and Applications* (Plenum Press, New York, 1981).
- [28] C. N. Yang, *Phys. Rev.* **74**, 764 (1948).
- [29] T. Gustafsson and H. J. Levinson, *Chem. Phys. Lett.* **78**, 28 (1981).
- [30] M. E. Smith, V. McKoy, and R. R. Lucchese, *J. Chem. Phys.* **82**, 4147 (1985).
- [31] P. J. Cumpson and M. P. Seah, *Surf. Interface Anal.* **18**, 345 (1992).
- [32] R. R. Lucchese *et al.*, *Phys. Rev. A* **65**, 020702 (2002).